Supplemental Material for the Manuscript: Decoupling the Cortical Power Spectrum Reveals Real-time Representation of Individual Finger Movements in Humans

Kai J. Miller[1], Stavros Zanos[2], Eberhard Fetz[2], Marcel den Nijs[1], Jeffrey G. Ojemann[3]
Departments of Physics[1], Physiology and Biophysics[2], and Neurological Surgery[3] ,
University of Washington, Seattle, Washington 98195, U.S.A.
(Dated: January 14, 2009)

This is a supplement for the paper titled "Decoupling the Cortical Power Spectrum Reveals Real-time Representation of Individual Finger Movements in Humans". There is a methods section, followed by supplemental figures which reinforce the primary text, and provide a deeper illustration for the more involved reader.

I. SUPPLEMENTAL METHODS

A. Experimental Protocol

1. Subjects

All 10 subjects in the study were epileptic patients at Harborview Hospital in Seattle, WA (18-45 years old, 6 female). Sub-dural grids were placed for extended clinical monitoring and localization of seizure foci. Each subject gave informed consent to participate in an internal-review-board (IRB) approved experimental protocol. All patient data was anonymized according to IRB protocol, in accordance with HIPAA mandate. Stimulation mapping was performed clinically, and coarse stimulation schematics were made available to the researchers (Fig. S11). All data and patient information was anonymized before handling by researchers.

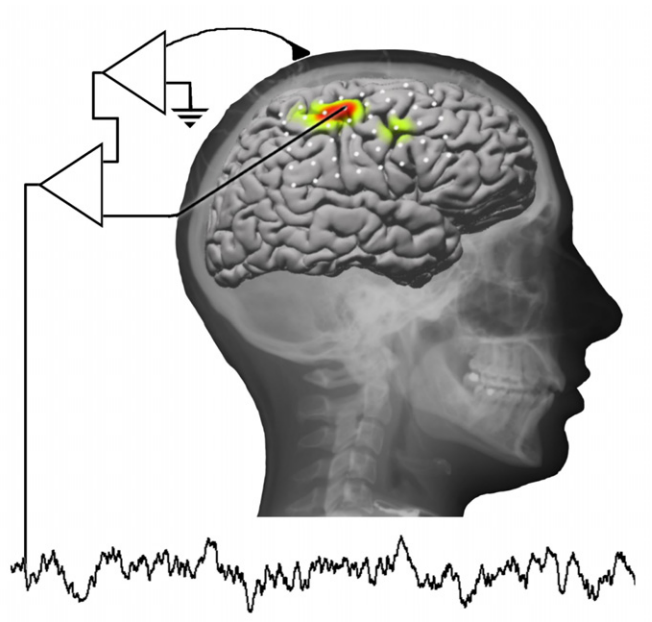

Figure S1: Potentials $V_n^0(t)$ were measured with respect to a scalp reference and ground before re-referencing with respect to the common average.

2. Recordings

Experiments were performed at the patients' bedside, using Synamps2 amplifiers (Neuroscan, El Paso, TX) in parallel with clinical recording (BMSI amplifiers for subjects 2, 4, 7, and xltek for all others). Stimuli were presented with a monitor at the bedside using the general purpose BCI2000 stimulus and acquisition program (interacting with the proprietary Neuroscan software), which also recorded and recorded the behavioral parameters and cortical data.

Sub-dural platinum electrode arrays (Ad-Tech, Racine, WI), with 32-64 contacts were arranged in 8x[4-8] arrays. The electrodes had 2.3mm diameter exposed surface, separated by 1 cm inter-electrode distance, and embedded in a silastic sheet. Cortical potentials were sampled at 1000 Hz, with respect to a scalp reference and ground (Fig. S1) .These signals had a software-imposed band-pass filter from 0.15 to 200 Hz, although the resultant higher frequency roll-off was corrected for attenuation after calculating the power spectral density (see below).

3. Cortical stimulation mapping

In five of the patients, cortical stimulation mapping [1] of motor cortex was performed for clinical purposes. Each such stimulation patient underwent stimulation mapping to identify motor and speech cortices to obtain a surgical margin as part of his/her clinical care. In this mapping, 510 mA square wave current pulses (2 ms period - 500Hz) were passed through paired electrodes for up to 3 s (less if positive finding) to induce sensation and/or evoke motor responses (Fig. S11).

4. Finger Movement task

During the finger movement task, subjects were cued with a word displayed on a bedside monitor indicating which finger to move during 2-second movement trials

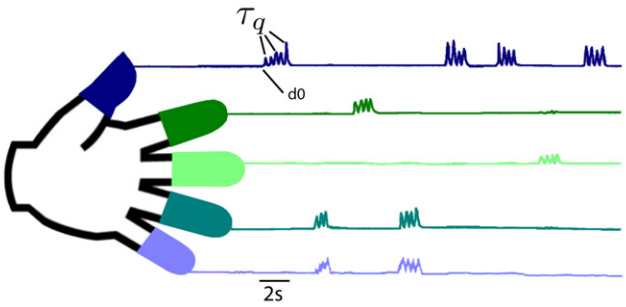

Figure S2: Capturing Individual finger movement times: Individual fingers were moved several times in response to each visual cue, and position was recorded using a dataglove. The peak displacement of each finger movement was marked with an event marker, τ_q (e.g. black arrow). The beginning and end times of each movement were also marked. Event markers, to characterize non-movement spectra for the "rest state" were chosen at random times at least one-half second from any movement event, and one-quarter second from each other. The onset of the first movement of type in response to a visual cue is denoted by $d0$. The ring (4^{th}) finger was not assessed after the PCA process because it's movements were always correlated with middle (3^{rd}) or little (5^{th}) finger movement.

(Fig. S2). The subject performed self-paced movements in response to each of these cues, and they typically moved each finger 3-5 times during each trial, but some trials included many more movements. A 2-second rest trial (blank screen) followed each movement trial. There were 30 movement cues for each finger (except subjects 4 and 7, whose trials were terminated after about 20 movement cues per digit), and trials were interleaved randomly. Finger position was recorded using a 5 degree-of-freedom dataglove sensor (5dt, Irvine, CA). Event markers were calculated marking the initiation, peak (denoted τ_q), and termination of each movement. This typically yielded 100-150 movements for each finger. Rest events (included in τ_q) were defined during random periods occurring at least 500 ms from any movement initiation or termination, and separated by at least 250 ms from any other rest event. There were typically 150-250 rest events for each subject. A 37ms ($\pm$ 3ms, SEM) lag occurred between the dataglove position measurement recording and the amplifier measurement and was accounted for when calculating the latency between brain activity and finger movement.

B. Spectral Analysis

1. *Calculation of samples of power spectral density*

Electrocorticographic (ECoG) sub-dural potentials, $V_n^0(t)$, were measured with respect to a reference and ground from the scalp, as in Fig. S1. These potentials were then re-referenced with respect to the common average reference across all N electrodes:

$$V_n(t) = V_n^0(t) - \frac{1}{N}\sum_{m=1}^{N} V_m^0(t) \tag{1}$$

A more local re-referencing of some type might produce slightly different (or perhaps, in some contexts, desired) results, but, in this setting, they would also inject the hypothesis and known spatial properties of the rhythms into the technique itself. Thus the common average reference was used to ensure that the decoupling process was naive. A set of epochs of duration T surrounding the time of maximum finger flexion, τ_q, were extracted from each timeseries $V_n(t)$, (Fig. S3 A). The epochs were sorted according to movement type q, and labeled by their event markers τ_q. The power spectral density (PSD) of each epoch was calculated as

$$P_n(f,q) = \left| \frac{1}{\sqrt{T}} \sum_{t=-\frac{1}{2}T}^{+\frac{1}{2}T} S(f,t) V_n(\tau_q + t)\, H(t) \right|^2 \tag{2}$$

with Hann window [2] $H(t) = \frac{1}{2}\left(1 + \cos\left(\frac{2\pi t}{T}\right)\right)$, in period $\tau_q - \frac{1}{2}T < t < \tau_q + \frac{1}{2}T$ and sinusoid $S(f,t) = \exp\left(i\frac{2\pi}{T}(f-1)t\right)$ as illustrated in Fig. S3 B-C. The lower bound of spectral consideration in this study, at 5Hz, was chosen to be above the frequency of finger movement, to avoid confounding rhythmic cortical phenomena with modulation correlated to rhythmic finger movement. The upper bound of 200Hz was chosen because of the amplifier's low-pass filter had a corner frequency there.

2. *Principal Component Decoupling of Power Spectral Density Samples*

The samples of the PSD, $P_n(f,\tau_q)$, were normalized in two steps prior to decomposition. First, each sample was normalized with respect to the average spectrum. This was necessary because the power law form of the PSD means that most of the variance, before normalization, is accounted for by the lower frequencies. Second, the log was taken. This places the ratios between 0 and 1 (-infinity to 0 after log) on equal footing with ratios between 1 and infinity (0 to infinity after log), see Fig. S3 D.

$$\tilde{P}(f,\tau_q) = \ln\Big(P(f,\tau_q)\Big) - \ln\Big(\frac{1}{N_q}\sum_{p=1}^{N_q} P(f,\tau_p)\Big) \tag{3}$$

(We drop the channel label, n, for brevity.) The label q refers to times of peak movement for all finger movement types, and times of "rest" where no movement was taking place.

The time ordering of the N_q epochs is explicitly ignored. In that case, the epochs represent an ensemble of N_q independent measurements of the underling power

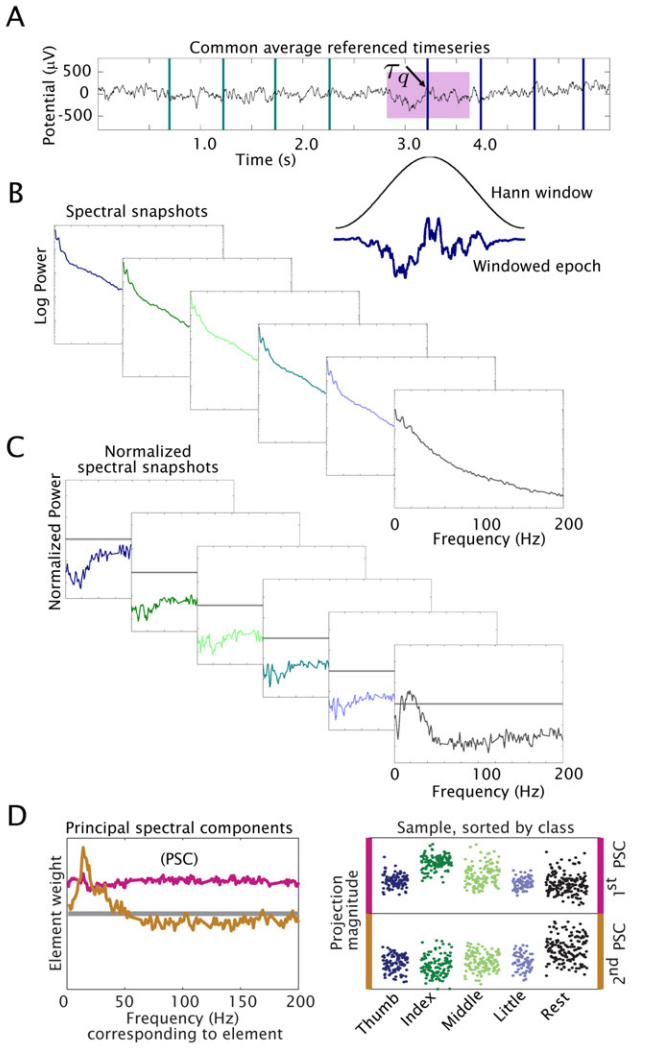

Figure S3: Signal Processing Steps: **(A)** The common averaged referenced signal, $V_n(t)$, is shown with event markers. The colors of the event markers distinguish between fingers, as in Fig. S2. A 1 sec Hann widow $H(t)$centered at each event marker, is imposed on the data to select the epoch corresponding to that specific event marker. **(B)** Samples of the power spectral density (PSD, $P_n\,(f,\tau_q)$) associated with each event marker are obtained for each epoch by Fourier transformation. **(C)** Each individual epoch power spectrum is normalized as described in the text, and the Principal Component method is applied to the logarithm of these normalized spectra. **(D)** Principal Spectral Components (PSCs, $\vec{e}_k$) are calculated across these across these sets of epoch power spectra $\log(\tilde{P}_n(f,\tau_q))$ (Left panel). The first is primarily flat across all frequencies (pink, $\vec{e}_1$), and the second is peaked in the classic α/β range (brown, $\vec{e}_2$). This structure is highly conserved, as shown in figure 2A of the main text. The panel on the left shows back projections of the first PSC (upper - pink, $W\,(1,\tau_q)$) and second PSC (lower - brown, $W\,(2,\tau_q)$) to the power spectral density samples, sorted by class. Note that the first PSC is specific for forefinger, and the second shows significant decrease for all movement classes with respect to rest (consistent with ERD).

spectrum $\tilde{P}(f)$ during the different types of finger movement. That power spectrum might include several distinct features that fluctuate with movements; in our case, the $\alpha\&\beta$ superimposed on the underlying broad band power law shape. The PCA method [3] attempts to identify the robust common features in such ensembles and decompose them by diagonalizing the second moment tensor of the corresponding distribution function, i.e., it determines the eigenvalues λ_k and eigenvectors $\vec{e}_k$ of the matrix

$$C(f,\tilde{f}) = \sum_{\tau_q} \tilde{P}(f,\tau_q)\tilde{P}(\tilde{f},\tau_q) \tag{4}$$

We intentionally center the covariance measure with respect to the log of the mean spectrum, rather than to the mean of log spectra. These eigenvectors, $\vec{e}_k$, the "Principal Spectral Components" (PSCs), reveal which frequencies vary together. They are orthogonal vectors, because $\hat{C}$ is a symmetric, $N_f \times N_f$ dimensional matrix. We normalize them, and order them according to the eigenvalues as $\lambda_1 > \lambda_2 > \cdots > \lambda_{N_f}$. The PSC's with largest λ's are the most significant ones. (Note that the variances are not normalized; a large λ reflects a large contribution to the total signal, and less likely to be a weak component with large within-movement-type fluctuations).

The PSCs represent a new orthogonal basis in frequency space. If we define the rotation matrix $A(f,k) = \left(\vec{e}_1, \vec{e}_2, \cdots, \vec{e}_{N_f}\right)$, then the projection, $W(k,\tau_q)$, of each individual original spectrum in the ensemble onto the new basis vector k is

$$W(k,\tau_q) = \sum_f A(k,f)\tilde{P}(f,\tau_q) \tag{5}$$

as illustrated in Fig. S3D. The inverse rotation matrix $\hat{A}^{-1}$, $\hat{A}^{-1} * \hat{A} = \hat{I}$, allows us to compare and visualize specific PSC components with the original full spectrum in frequency space (for each member of the ensemble),

$$\tilde{P}_k(f,\tau_q) = \sum_f A^{-1}(f,k)W(k,\tau_q) \tag{6}$$

The classic peaked rhythms are typically accounted for by the 2^{nd} and 3^{rd} PSCs. Therefore we define the "μ-rhythm" (low frequency peak) back-projection as

$$\tilde{P}_\mu(f,\tau_q) = \sum_{k=2,3}\sum_f A^{-1}(f,k)W(k,\tau_q) \tag{7}$$

and we associate the complement with the power-law like broad band

$$\tilde{P}_{pl}(f,\tau_q) = \sum_{k\neq 2,3}\sum_f A^{-1}(f,k)W(k,\tau_q) \tag{8}$$

The 1^{st} PSC on its own, $\tilde{P}_1(f,\tau_q)$, typically reconstructs most of the power law shape.

C. Time-Frequency approximation (Dynamic Spectrum)

Time-Frequency approximations (dynamic spectra) were made using a wavelet approach. In this way, a

time-varying Fourier component $\tilde{V}(t,f)$ (channel label dropped) is obtained at each Hz, with fixed uncertainty between the estimate of the instantaneous amplitude and phase vs. the temporal resolution. The projection of each principal spectrum can then be estimated at each point in time.

1. Wavelet

A wavelet [4] of the form: $\psi(t,\tau) = \exp\frac{i2\pi t}{\tau}\exp\frac{-t^2}{2\tau^2}$ is convolved with the timeseries to get a time-frequency estimate for every $f = 1/\tau$:

$$\tilde{V}\left(t, 1/\tau\right) = \sum_{t'=-5\tau/2}^{5\tau/2} V(t+t')\psi(t',\tau) \tag{9}$$

A total of 5 cycles is used to estimate the amplitude and phase of the signal at each frequency for every point in time.

2. Movement-triggered average of time-frequency power estimate

This time-frequency approximation can be used to calculate mean power in relation to the onset of each type of digit movement:

$$\overline{P}^d(f,t) = \frac{1}{N_{d0}}\sum_{\tau_{d0}}\left(\frac{\left|\tilde{V}(t+\tau_{d0},f)\right|^2}{\frac{1}{T}\sum_{t'=1}^{T}\left|\tilde{V}(t',f)\right|^2}\right) \tag{10}$$

Where $d0$ is the first movement of type d in response to the visual cue (Fig. S2). These normalized maps of power as a function of time and frequency provide important information about characteristic spectral changes with local cortical function, as shown in figure 1 of the main text and figures S8, S12, and S14 of this supplement.

3. Wavelet projection to the 1st PSC

The time course of each PSC, $W^c(k,t)$ (c denotes continuous) can be estimated from the wavelet type, time-varying, estimate of the power spectral density (using the same normalization as in equation 3),

$$P^{(n)}(f,t) = \ln\left(\frac{\left|\tilde{V}(t,f)\right|^2}{\frac{1}{T}\sum_{t=1}^{T}\left|\tilde{V}(t,f)\right|^2}\right) \tag{11}$$

by projecting

$$W^c(k,t) = \sum_f A(k,f)P^{(n)}(f,t) \tag{12}$$

We apply this to the first PSC. Recall that the 1^{st} PSC captures a broad change across the entire frequency range. Our previous attempts to capture this phenomenon dubbed it the so-called χ-band or χ-index feature, as it was an attempt to capture the power law phenomenon, $P \sim Af^{-\chi}$, with exponent χ. Here we will call attempts to capture it in real-time, $C_1(t)$, which is an attempt to capture fluctuations in the coefficient, A, of the power law phenomenon. We calculate it first by projecting to W^c, smoothing with a gaussian (SD=15ms), and then normalizing and re-exponentiating, so that

$$C_1(t) = \exp\left(\frac{W_s^c(1,t) - \overline{W_s^c(1,t)}}{\sigma\left(W_s^c(1,t)\right)}\right) \tag{13}$$

Where W_s^c is a smoothed version of W^c, σ denotes the standard deviation, and the overline denotes the mean. The dynamics of $C_1(t)$, with finger movement, are shown in figures 2 and 4 the main text. Because of the high correlation between behavioral parameters and $C_1(t)$ in specific electrodes, we propose that $C_1(t)$ can be used generically as a correlate of local cortical function.

4. Back-projection from PSC to time-frequency power

The constrained back-projection matrices, $\hat{A}_{pl}^{-1}$ and $\hat{A}_{\mu}^{-1}$ (defined in equations 8 and 7), were applied to $W^c(k,t)$ to obtain time-frequency estimates, $P_{pl}(f,t)$ and $P_{\mu}(f,t)$ of the power change:

$$\hat{P}_{pl} = \exp\left(\hat{A}_{pl}^{-1} * W^c\right) \tag{14}$$

$$\hat{P}_{\mu} = \exp\left(\hat{A}_{\mu}^{-1} * W^c\right) \tag{15}$$

Event-averaged (in the same way as equation 10), constrained, back-projections are demonstrated in figure 1 of the main text and figures S9 and S12 of this supplement.

5. Movement-onset to phase relationship

Figure S14 shows the relations between the phase $\theta(t,f)$ and magnitude of the complex signal, $\tilde{V}(f,t) = |\tilde{V}(f,t)|e^{i\theta(f,t)}$ in terms of polar plots, i.e., by plotting the real and imaginary parts of $\tilde{V}(f,t)$ along the x respectively y-axis.

The relationship of the phase of the complex signal $\tilde{V}(t,f)$ to the onset of finger movement can be examined by examining the average phase vector at each frequency, with respect to the first movement of each cue of each type, for each point in time, with respect to each cue.

If the complex form of $\tilde{V}(t,f)$ is expressed as $\tilde{V}(t,f) = x(f,t) + i\, y(f,t)$, then the unit magnitude phase vector at a given time and frequency is:

$$\vec{\phi}(f,t) = \frac{x(f,t)\ \hat{x} + y(f,t)\ \hat{y}}{\sqrt{\left(x(f,t)\right)^2 + \left(y(f,t)\right)^2}} \tag{16}$$

The average phase vector, with respect to the first movement of type d, denoted $d0$ from each cue.

$$\vec{\phi}^{\,d}\,(f,t) = \frac{1}{N_{d0}} \sum_{\tau_{d0}} \vec{\phi}(f, t+\tau_{d0}) \tag{17}$$

6. *Trace of high frequency band power*

We calculate a trace of of the high-frequency band (76-100Hz) power, $H(t)$ of our previous paper [5], because it may be of interest to some readers to compare it to $C_1(t)$. The raw filtered power is smoothed and normalized in the same manner as $C_1(t)$ using the following prescription: We begin by filtering the common-average referenced signal for the 76-100Hz range using a Butterworth filter, and then squaring it to obtain the high frequency power: $H^0(t) = \left(V(t)\right)^2$. Then it's log is taken, and it is smoothed by with a gaussian (SD=15ms, smoothed $ln(H^0(t))$ is denoted $H_s(t)$). Then it is normalized and re-exponentiated:

$$H\,(t) = \exp\left(\frac{H_s(t) - \overline{H_s(t)}}{\sigma\left(H_s(t)\right)}\right) \tag{18}$$

Where σ denotes the standard deviation and the overline denotes the mean. The temporal character of $H(t)$ is compared with $C_1(t)$ in figure 15. It shows that this trace is a "reasonably good" approximation of $C_1(t)$, which may be more practical to obtain in many experimental settings, where decoupling the spectrum and isolating broadband change is not appropriate.

II. SUPPLEMENTAL FIGURES

How can we measure population-scale neural dynamics in the brain, at timescales relevant to behavior? In the primary text, titled "Decoupling the Cortical Power Spectrum Reveals Individual Finger Representation in Humans" we demonstrate a new method of extracting and removing the low frequency α and β rhythms to reveal a behaviorally modulated broadband signal in the ECoG power spectrum. This signal provides significantly improved spatial resolution of localized cortical populations, with high (<20ms) temporal resolution. In the supplemental figures below, we present material which reinforces the primary findings of the text, and also provide a more broad illustration of the experimental settings for the involved reader.

Previous studies have demonstrated that, in motor cortex, there is a reliable increase in spectral power at high frequencies (>60Hz), and decrease in spectral power at low frequencies (<40Hz), with movement. In our manuscript, we characterize, and decompose, these changes during a finger movement task (shown across all 10 subjects, in Fig. S4, and the time-frequency decomposition across the whole ECoG array in a single subject, in Fig. S8). These characteristic spectral changes are not simply due to an event-related potential, as illustrated in Fig. S14. Changes in spectral power were shown to be naively separable into two basic motifs. Band-specific decreases in power in the low frequency range were separable from broad spectral changes across all frequencies. Figure 1 of the main text demonstrated this in a single electrode, and Fig. S4 of the supplement demonstrates that this finding generalizes across all subjects and electrodes in this study. The decoupling of these two phenomena, as applied to the dynamic time-frequency spectrum, is shown for different finger movement types, in adjacent electrodes, in Figs. S8 and S9. The isolated low frequency change has been hypothesized to reflect synchronization and desynchronization of cortical processes. The broad spectral change, however, has no specific timescale, and is more consistent with fluctuations in a noise-like power law. As shown in Fig. S12, the types of characteristic changes associated with the 2^{nd} and 3^{rd} principal spectral component (PSC) motifs may reflect populations of inputs to a cortical area which are distant, rhythmic, and synchronous. The 1^{st} PSC, in contrast, may reflect asynchronous superposition of many Poisson-distributed spiking inputs which are local in nature; because they are not correlated at any specific timescale, they are revealed by changes in a broadband, power-law ($P \sim Af^{-\chi}$), process.

These two types of processes had very different specificities for different finger movements. The 1^{st} PSC showed specific, somatotopic, increase for single finger movement types, that was coincident with cortical stimulation (Fig. S11) and located in the expected pre-central cortical areas (Figs. S5 and S10), while the 2^{nd} PSC showed a much less specific decrease for all finger movement event types, compared with resting. Fig. S5 shows this somatotopy, while Fig. S6 illustrates that the finger representation for the 1^{st} PSC is much less distributed (more specific and more sparse) than that of the 2^{nd} PSC. The projection of the time-frequency spectrum to the 1^{st} PSC ($C_1(t)$), demonstrates that not just the movement triggered events are specific for individual fingers, but that the dynamics are specific as well (Fig. 7). The cases where finger representations were less well demarcated by this movement-related, principal-component, decomposition, were the same cases where the movement behavior was not well demarcated (Fig. S13).

[1] Ojemann, 1982; Ojemann et al., 1989; Chitoku et al., 2001

[2] in "Particular Pairs of Windows." published in "The Measurement of Power Spectra, From the Point of View of Communications Engineering", New York: Dover, 1959, pp. 98-99.

[3] Principal Component Analysis, IT Joliffe - 1986 - Springer-Verlag

[4] P. Goupillaud, A. Grossman, and J. Morlet. Cycle-Octave and Related Transforms in Seismic Signal Analysis. Geoexploration, 23:85–102, 1984

[5] Miller, K.J., et. al. Journal of Neuroscience, 2007

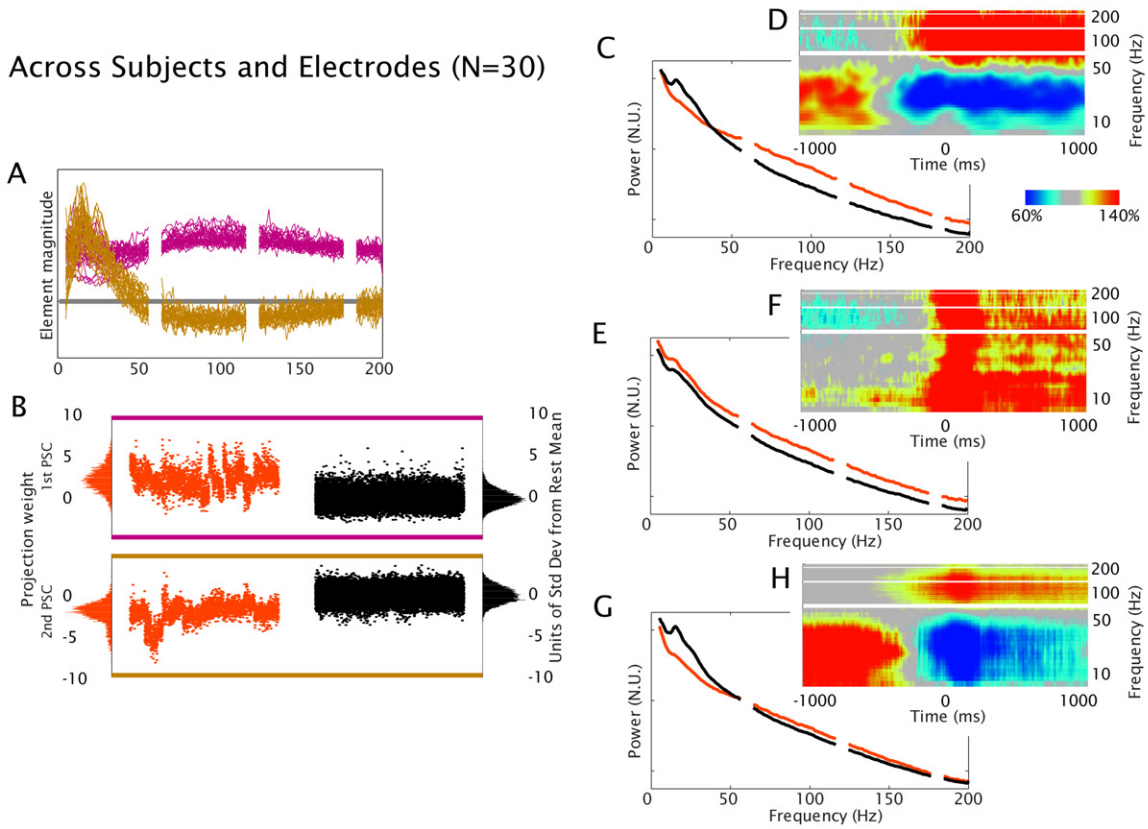

Figure S4: **Representative spectral changes across all subjects:** Data are from all 30 electrodes, (10 subjects, 3 electrodes each), where one movement type (thumb, index, little) was paired with each electrode (indicated by color code in figures 2, 3 and S4-10). **(A)** All 1^{st} (pink) and 2^{nd} (gold) PSCs, normalized by area, demonstrate the same structure for all subjects and electrodes. Note that the expected residual variance between the two phenomena is reflected by the small negative residual weight in the 2^{nd} PSC above 50Hz. **(B)** All of the projection magnitudes of the PSCs from (A) for the paired-movement type (orange, indicating thumb, index, or little finger movement samples, corresponding to the specificity of each electrode) and rest (black), flanked by the appropriate probability density functions. The plots are in units of standard deviation from the mean of the projection weight of rest samples. **(C)** The normalized mean PSD, averaged across subjects and electrodes (Power in normalized units (by mean power above 55Hz): "N.U."), of paired-movement samples (orange, corresponding to the appropriate movement for each electrode) and rest samples (black). **(D)** The averaged time-varying PSD (geometric mean, scaled as % of mean power at each frequency) with respect to first paired-movement from the associated cue (N=29-33, per electrode). **(E)** Mean of reconstructed PSD samples, omitting the 2^{nd} and 3^{rd} PSCs. Power goes up with movement at all frequencies, consistent with the increase of the pre-factor, A, in a power law $P \sim Af^{-\chi}$. **(F)** Average reconstructed time-varying PSD, with 2^{nd} and 3^{rd} PSCs omitted. **(G)** Mean of reconstructed PSD samples, using only 2^{nd} and 3^{rd} PSCs. The decrease in power with movement is confined to peaks in the classic α/β rhythm range. **(H)** Average reconstructed time-varying PSD, from only 2^{nd} and 3^{rd} PSCs.

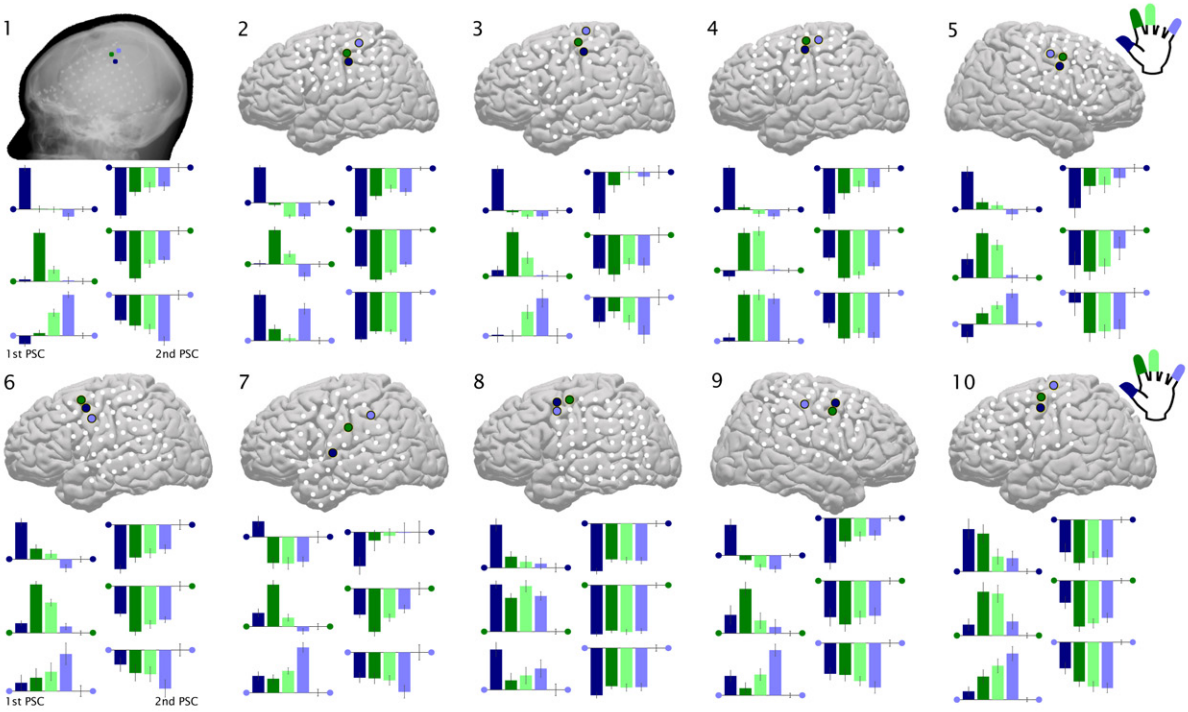

Figure S5: **Somatotopy for all individuals:** The mean projection magnitudes to samples of different finger movements for the first (left) and second (right) PSCs in subjects 1-10, with respect to the mean of rest samples. The colored dots flanking each axis correspond to the electrode that they reflect the activity of. The axis indicates the mean of rest period samples. The colors on the bars indicate the appropriate finger (from left to right: thumb, index, middle, little), and the 3σ error bars indicate +/- 3 times the standard error of the mean. The 3σ error bars on the right most portion of the axis are +/- 3 times the standard error of the mean of the rest period samples. The element weights of the first PSC are non-zero and roughly equal across all frequencies consistent with a power-law like change, where power at all frequencies fluctuates together, and this structure is highly conserved, as shown in figure 1A of the main text. The elements of the second PSC (gold) are peaked in the α / β / μ range, reflecting a process where just these frequencies vary together around a central frequency of peak importance (conserved as also shown in figure 1A). *The difference in the distribution in the two components is evident:* ***(1)*** The first PSC is specific for particular movement types, and the projection magnitude increases with respect to rest (therefore the power in the original power spectral samples). This is consistent with the spatial distribution of digits described by stimulation results (See the Penfield and Woolsey references of the main text). ***(2)*** The second PSC is non-specific, there is a decrease in projection magnitude for samples of each movement type with respect to rest samples. The qualitative gradient observed between movement types in the 2^{nd} PSC is consistent with more recent infarct and MRI studies (See the Dechent, Kim, Kleinschmidt, and Schieber papers of the main text). These two observations illustrate how it was possible to pull these apart because the classic, low-frequency, peaked phenomena decrease in power with local activity, and do so over a large spatial area. Since the representations of different fingers are close to each other, but distinct, the peaked phenomena and the power law phenomena vary in a separable way, and can therefore be decoupled using the principal component analysis method.
Observations about individual subjects: **(Subject 2)** The lower set of bars for the first PSC (light blue electrode) shows signifcant change vs. rest for both thumb and little finger samples. **(Subject 3)** 1st PSC - Note partial representation of middle finger along with both little and index fingers. 2nd PSC - In the dark blue electrode, only thumb samples are different from rest. **(Subject 4)** 1st PSC - Index and middle fingers are strongly represented in the dark green and light blue electrodes, but the little finger is only represented in the light blue electrodes. The correlation in the representation of the index and middle fingers may be due in part to the fact that the movements themselves were correlated, as shown in figure S13. **(Subject 5)** 2nd PSC - Conjugate observation: Little finger is not represented in the dark blue electrode, and thumb electrode is not represented in the light blue electrode. The correlation between index and middle finger may be due in part to movement correlation (figure S13). **(Subject 7)** The dark blue electrode was selected based upon statistics, but it is clearly not in motor area, and clearly different from any other in the study. It is likely in a pre-motor or supplementary area. In the 1st PSC, index, middle, and little finger movements samples are all decreased from rest samples, while thumb is increased. In the 2nd PSC, there is no significant change from rest, except for thumb movement. **(Subject 8)** The grid lies inferior to most of hand area, and the significant electrodes were all significant for thumb movement. The green electrode was significant for all types of finger movement samples.

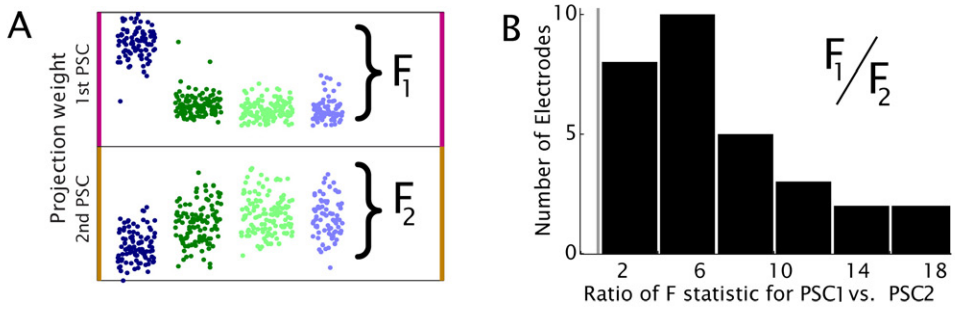

Figure S6: **Quantifying difference in sparse distribution of finger representation for the 1^{st} and 2^{nd} PSCs.** In order to demonstrate that the 2^{nd} PSC is less sparse than the 1^{st}, overall, an ANOVA was calculate for the distribution of different finger movements, for spectral sample projections to the 1^{st} PSC, and the 2^{nd} PSC, independently, as shown in **(A)**. Every electrode was significant at $p<.05$ for one or more finger movement types being different from the others. However, the more different one class is from the rest in an ANOVA, the larger the associated F-statistic will be, so the relative magnitudes of the F-statistics for the 1^{st} PSC and the 2^{nd} PSC in a single electrode will tell us about their relative sparsity . As shown in the histogram of ratios F_1/F_2 in **(B)**, every such ratio F_1/F_2 was greater than 1 (vertical gray line), demonstrating that the representation of the 1^{st} PSC is more sparse than the 2^{nd} PSC in every single case (N=30, 3 electrodes in 10 subjects).

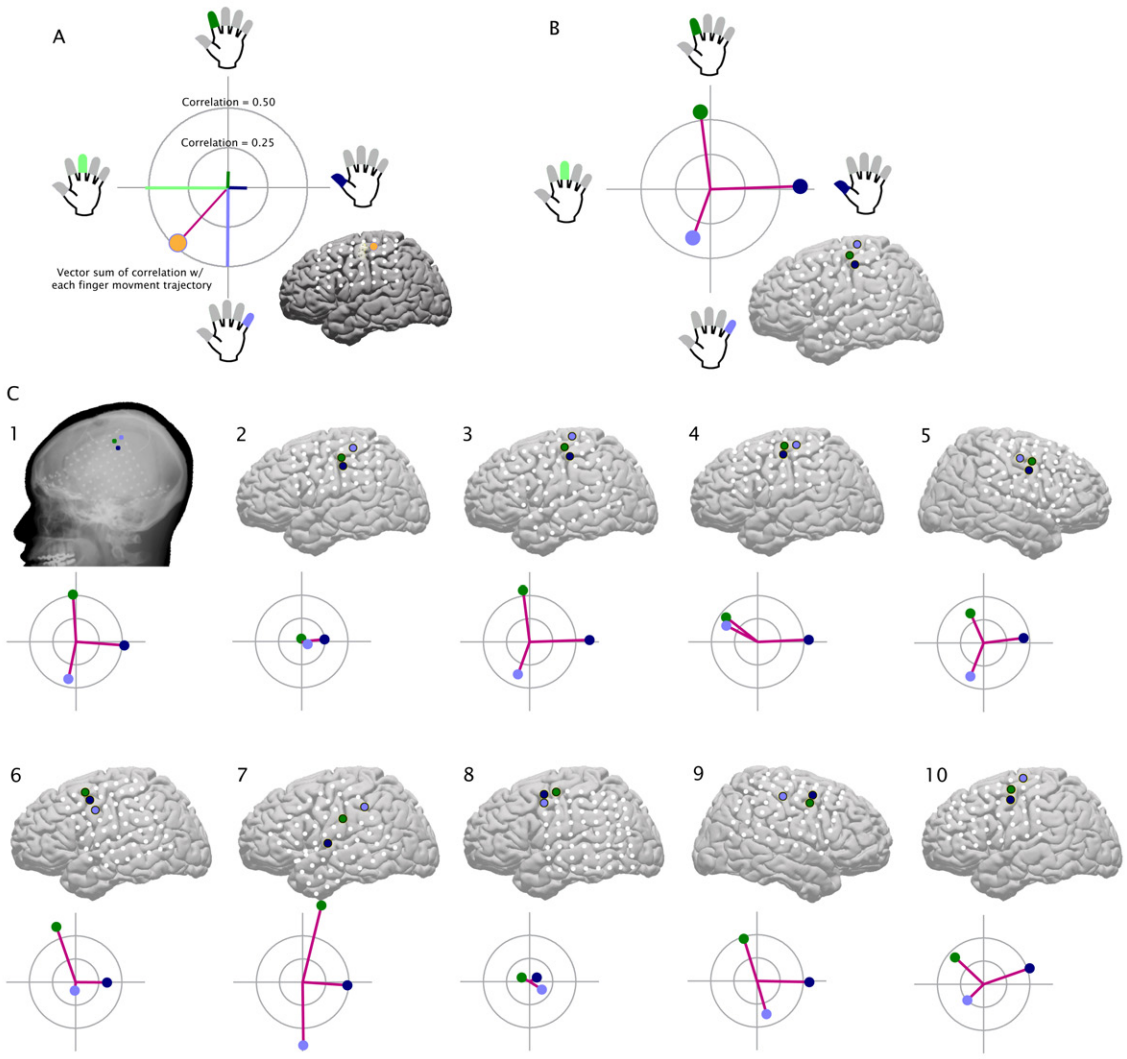

Figure S7: **Somatotopic cortical tuning for different fingers. (A)** *Cortical tuning plot schematic:* The correlation, r of $C_1(t)$ (projection of 1st PSC to the dynamic spectrum) with the finger position is projected on polar axes. The correlation with thumb position is shown at 0 deg, index finger at 90 deg, middle finger at 180 deg, and little finger at 270 deg. The vector sum of these is shown as a pink line with a color-coded dot at the end, denoting the appropriate electrode on the inset brain. The inner circle denotes a correlation of r=0.25, and the outer circle denotes a correlation of r=0.50. **(B)** Each of the three paired electrodes is shown on the same polar plot, for each subject. **(C)** For each subject (numbered 1-10), the appropriate cortical tuning plot is shown. All subjects except 2 and 8 were strongly tuned (for this reason, subjects 2 and 8 were excluded from the histogram and grand average shown in figure 4 of the main text).

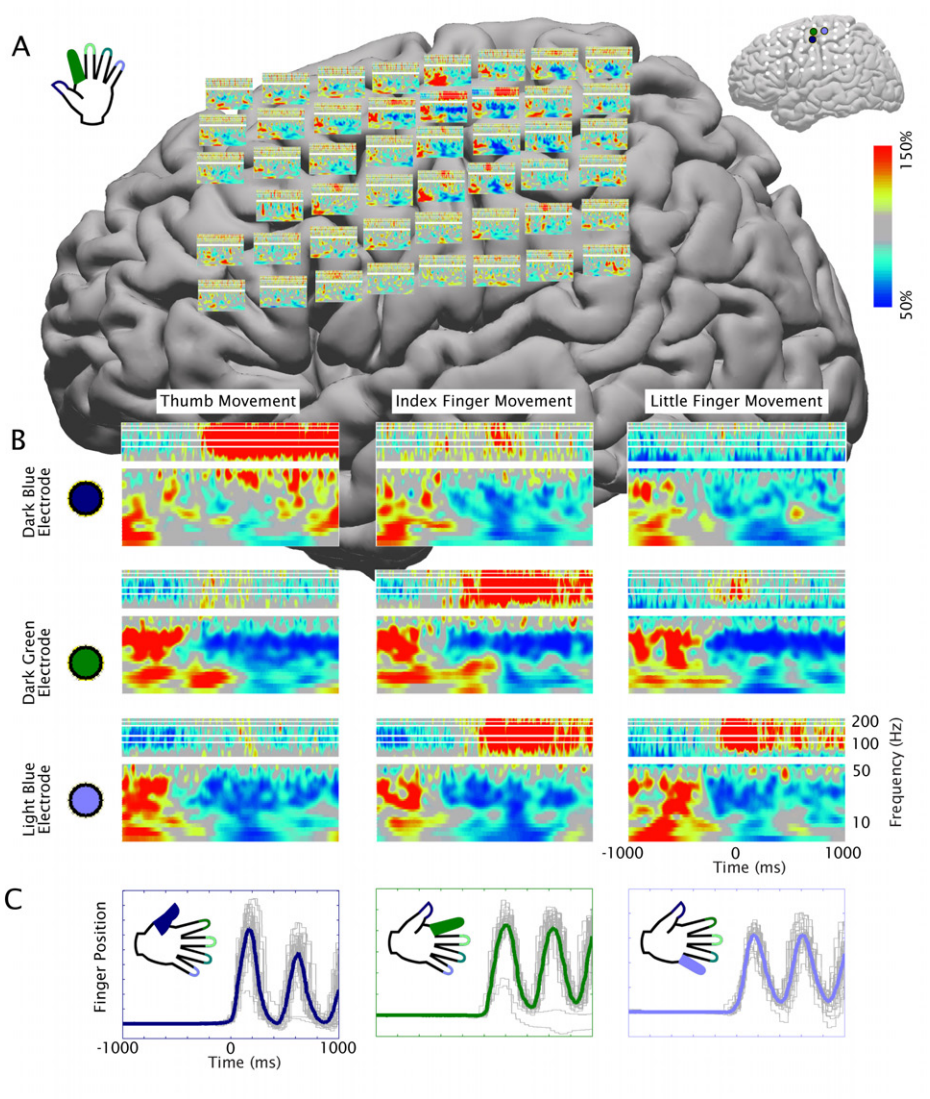

Figure S8: Time Frequency Plots for 3 adjacent electrodes and 3 different finger movements in subject 4. (A) Average time-varying PSD (scaled as % of mean power at each frequency) with respect to first index finger movement from each index finger movement cue (N=27), for each electrode, shown in the approximate position of the electrode that it corresponds to. The axes are scaled as detailed in the lower right of (B). Note that the decrease in lower frequencies prior to movement onset is predominant over a large area, but pronounced increase in power at high frequencies is limited to 2 electrodes. (B) The temporal development of the PSD is shown averaged over each of the three for each the three movement types most "relevant" for each of three electrodes (position shown in right of (A)). Note that all electrodes have characteristic decrease in power with movement onset in the low frequency range, and increase in power at higher frequencies is specific. These are fully decoupled with the principal component method, as shown in supplemental figure 9. (C) Average finger position, triggered to the onset of the first movement during the appropriate cue ("position" denotes arbitrary units of flexion).

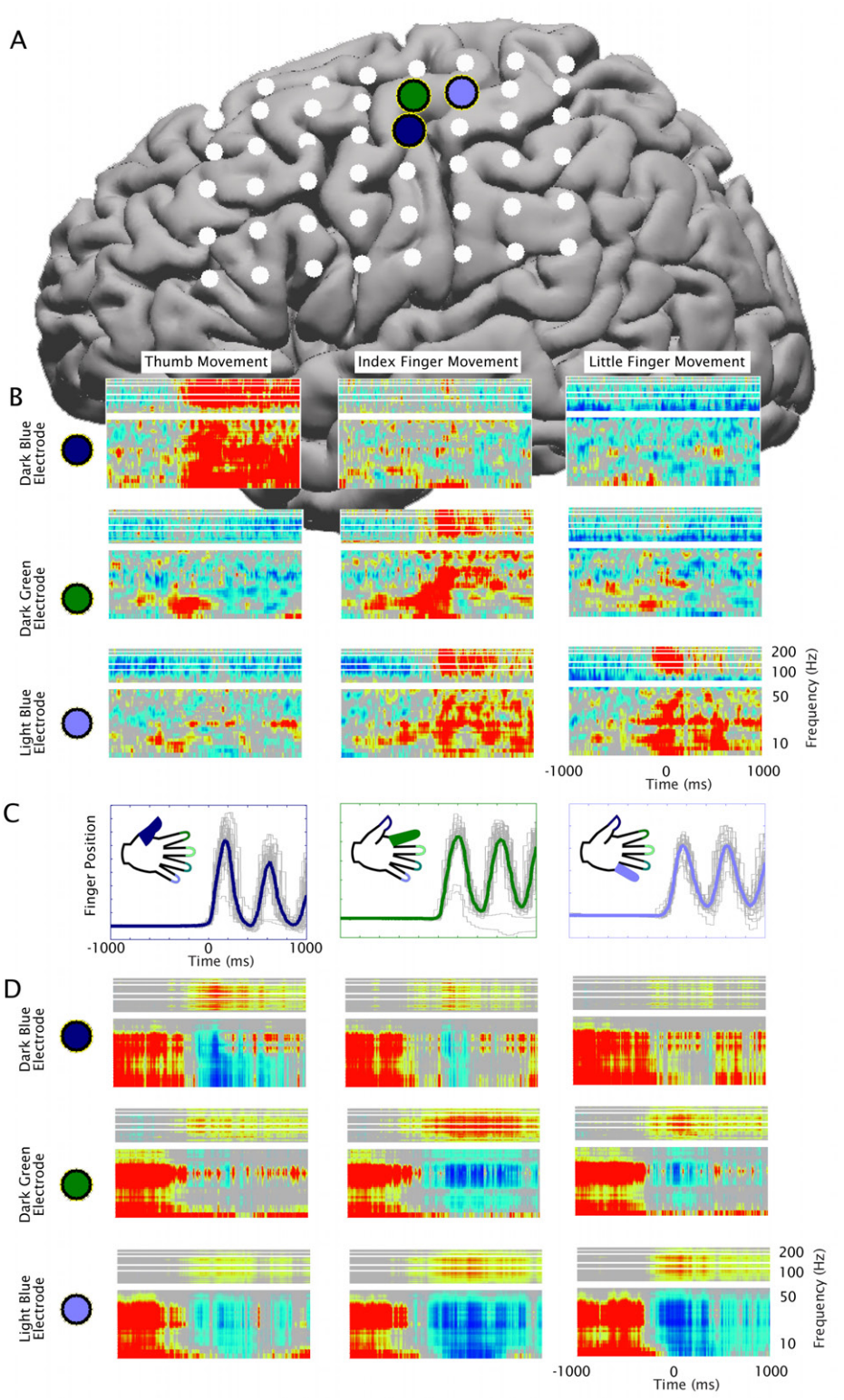

Figure S9: Several movements and several electrodes, decoupled: Decoupled time frequency plots from supplemental figure 8 . (D) shows the event-related desynchronization at lower frequencies, while (B) shows the more specific power law. (A) shows the electrode positions, and (C) shows the finger position.

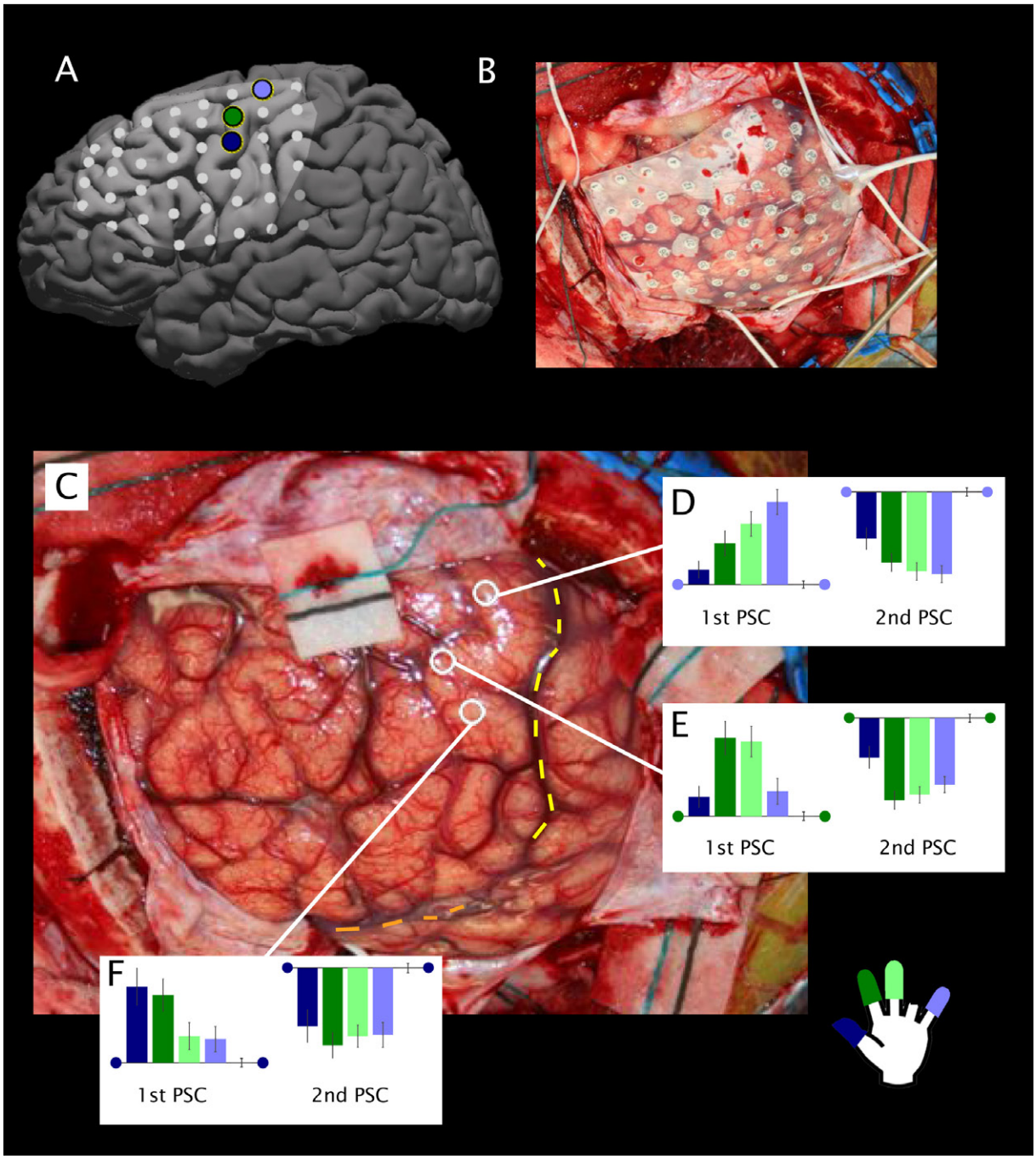

Figure S10: **Locations of electrodes on intra-operative surgical photograph. (A)** The interpolated locations of the three paired electrodes for subject 10. **B & C** In subject 10, a surgical photograph was taken, pre- and post- grid implantation. The sites of the 3 paired electrodes (**D-F**, as in supplemental figure S5.) could be identified on the cortical surface. They all lie in the classic pre-central hand area. *Yellow line denotes the central (Rolandic) sulcus, and the orange dotted line denotes the lateral (Sylvian) sulcus, left is rostral, right is caudal, up is dorsal, and down is ventral.* Although not the general case, the overlapping gradient observed between movement types, in this case, illustrates an occasion where the 1^{st} PSC is consistent with recent infarct and MRI studies (See the Dechent, Kim, Kleinschmidt, and Schieber papers of the main text).

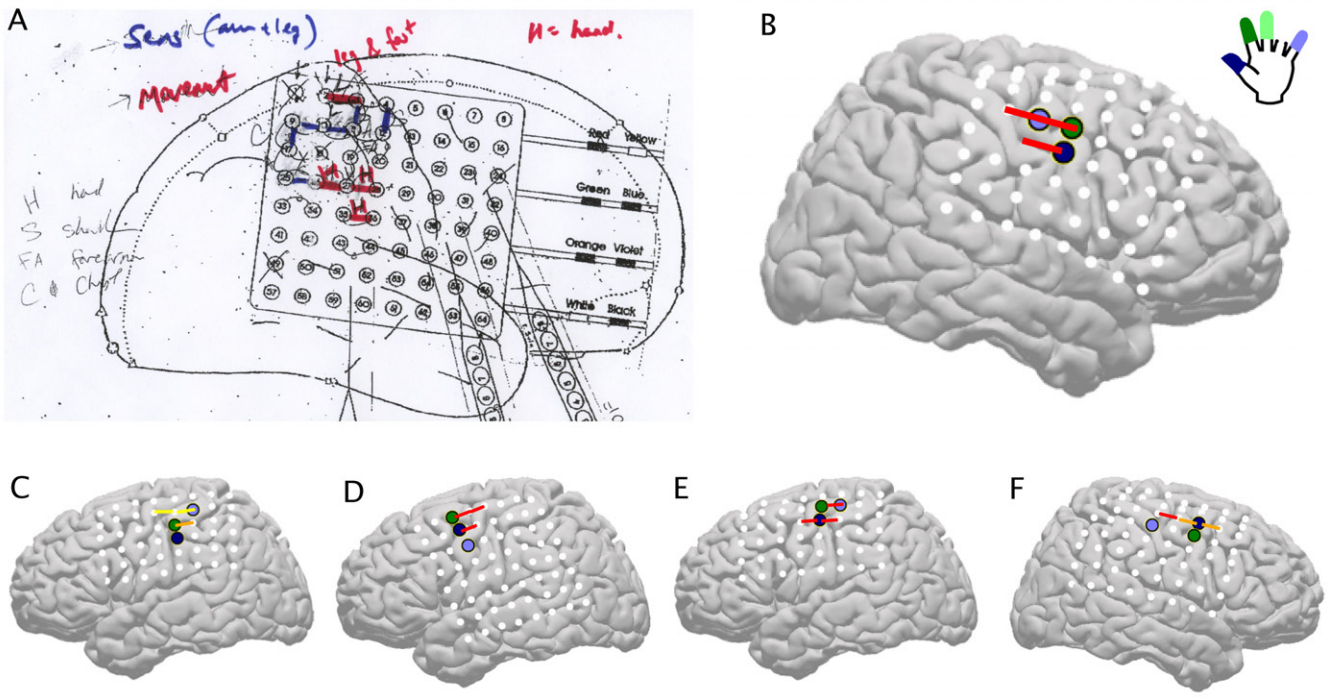

Figure S11: **Relation to clinical stimulation findings:** Clinical stimulation mapping was performed on a subset of the subjects. In each of the subjects, the clinical goal was to obtain an acceptable surgical margin, so not all of the electrodes were surveyed. Stimulation was performed pairwise. In two of the cases (subject 2 in (C) and subject 9 in (F)), the clinicians reported specific digit movement. In both of these cases, the specific movements reported were the same as the specific digit identified by the 1^{st} PSC. **(A)** Clinical schematic showing hand area in subject 5, note that there were both motor and sensory findings, and both hand and foot motor areas were identified. In all cases, electrodes connected by a red bar indicate a report of non-specific hand/finger movement. Because stimulation was pairwise, the assumption is that the area of cortex which produced the given motor phenomena was under one or both of the electrodes, or the cortex bridged by the pair, or a combination of all 3. **(B)** Subject 5. **(C)** Subject 2: Yellow bars indicate ring and little finger movement with stimulation; orange bar indicates little and middle finger movement with stimulation. Stimulation was not performed inferior (ventral) to these sites. **(D)** Subject 6. **(E)** Subject 4. **(F)** Subject 9: Orange bar indicates thumb movement with stimulation.

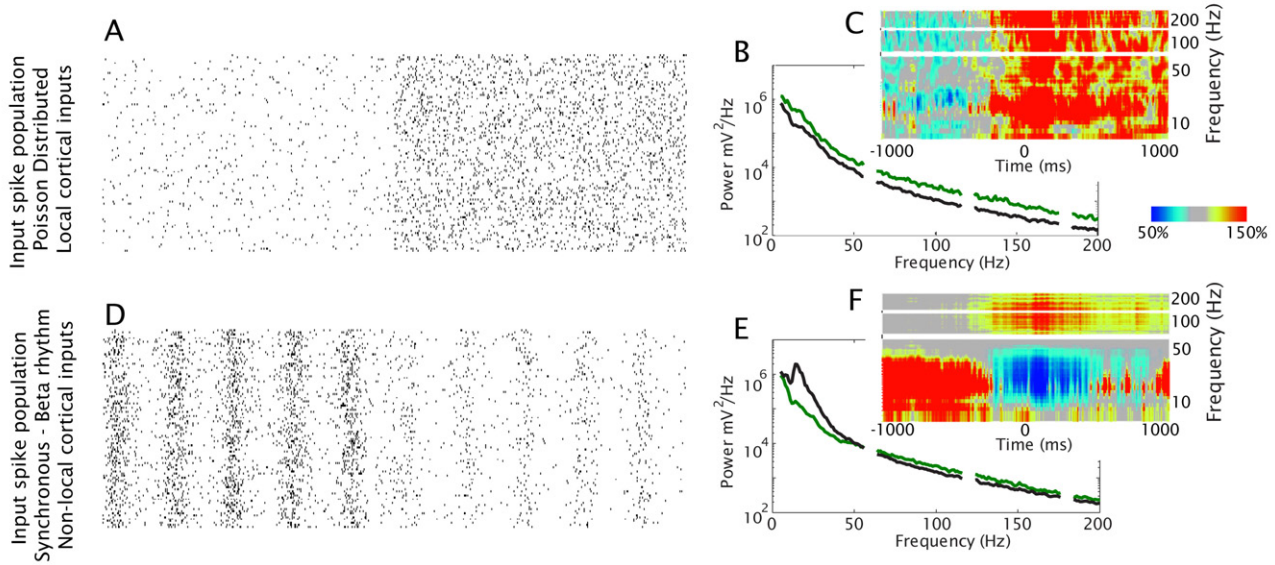

Figure S12: **Hypothetical input - spectral change relation: (A)** The power law changes we found are mathematically consistent with many superimposed Poission distributed input spikes, filtered by the shape of the post-synaptic potential. With an increase in local activity, the rates of these processes increase, and the corresponding power spectral changes, shown in **(B & C)** correspond to an increase in the coefficient, A, of a power law of form $P \sim Af^{-\chi}$. **(D)** The peaked changes we found are mathematically consistent with a set of synchronized input spikes with synchronous frequency in the β range. With activity, the synchronous activity dissipates, or perhaps remains constant but loses synchronous timing, which would be in contrast to the schematic here. The corresponding spectral changes for this type of process were found in our 2^{nd} and 3^{rd} Principal Spectral components, projected in **(E & F)**. Panels B, C, E, and F were taken from the single-electrode example in figure 1 of the main text.

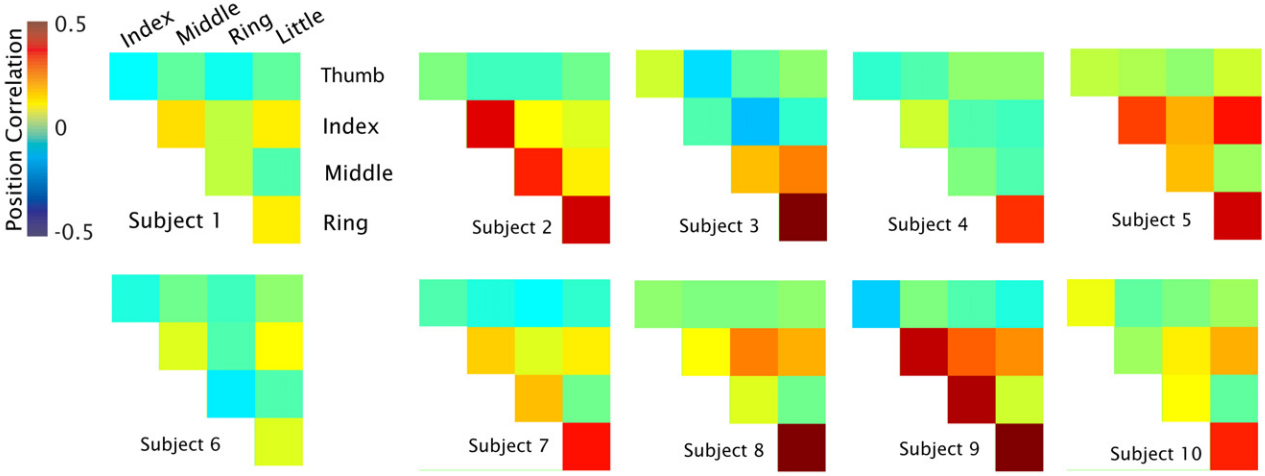

Figure S13: **Correlation between different digit movements:** Different finger movement traces were correlated to varying degree on a subject by subject status. Correlation displayed was capped at $\pm$ 0.5. This meant that individual spectral samples labled as one type of finger movement may actually have had movement for more than one type, and brain activity during these samples is really for both fingers together. Index often correlated with middle, and little often correlated with middle. The movement of the ring finger was highly correlated in every case with either little or middle fingers (depending on subject) - it was excluded from examination altogether after the PCA step was performed.

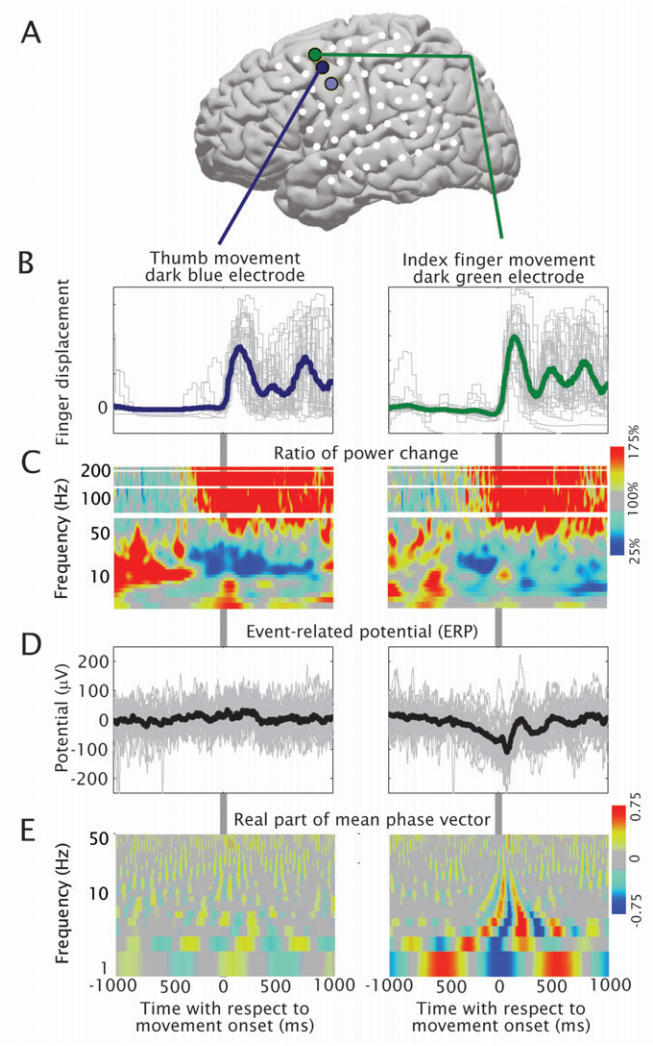

Figure S14: **Event-Related Potential:** Illustration that the characteristic changes in the power spectral density changes with activity are not due to an reproducible event related potential shift (ERP). Two adjacent electrodes in subject 6 are shown in **(A)**. One has an ERP, and one does not, but both have the characteristic peri-movement spectral changes. **(B)** Individual (grey) and averaged thumb movement (dark blue) or index finger movement (dark green), locked to the first movement from the appropriate movement cue. **(C)** The normalized power spectral density ("PSD") as a function of time. It demonstrates the classic spectral changes just prior to movement onset for both thumb and index finger. Note that the decrease in power at lower frequencies (α / β / μ range), and the increase in power at higher frequencies (above 40Hz) both begin before movement onset. **(D)** Individual and averaged raw potential traces around each of the first movements from appropriate thumb or index finger movement epochs. There is no significant stimulus event-related potential (ERP) effect for thumb, but there is for index finger. **(E)** Real part of mean phase vector at each point in time/frequency, locked to movement onset. The envelope of this is what would classically be called the "inter-trial coherence". It is not significant for the thumb task/electrode, but for the index finger task/electrode, this demonstrates evidence of "phase locking to stimulus" classically associated with the ERP.

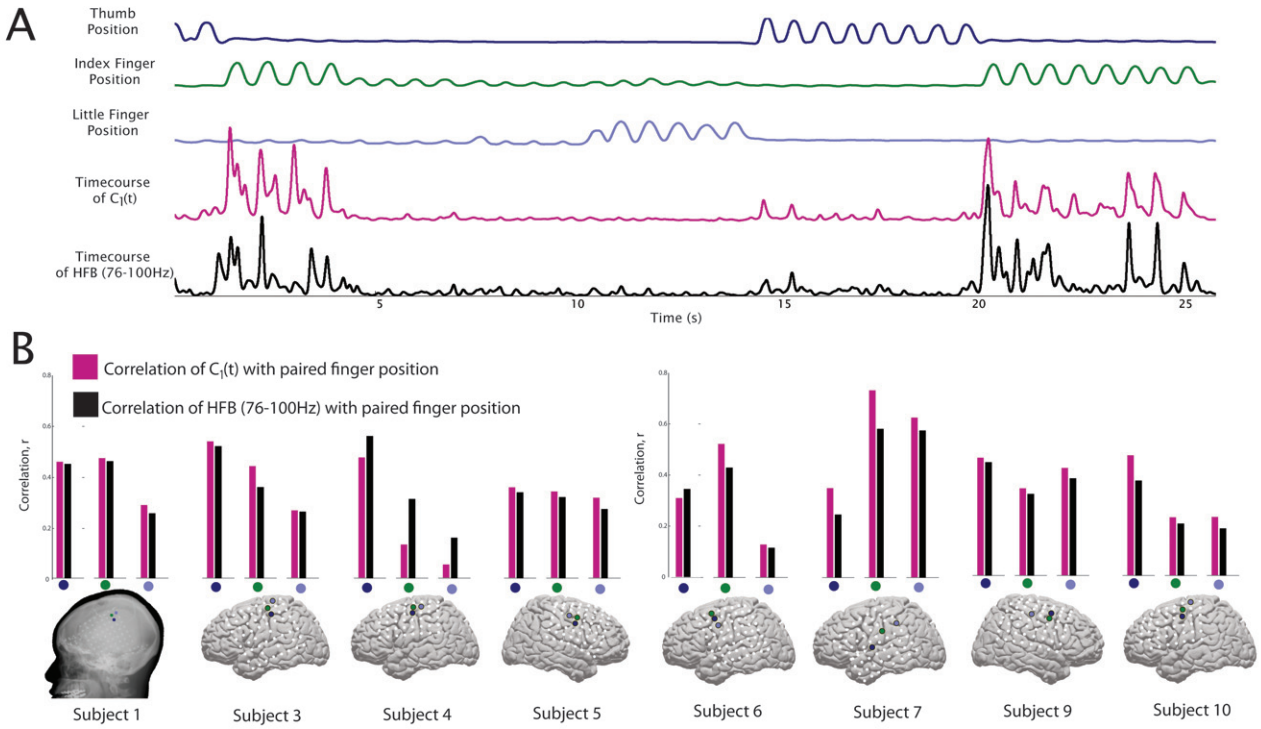

Figure S15: **The relation between filtered high frequency power and $C_1(t)$:** The high-frequency band power (76-100Hz), $H(t)$, is compared with $C_1(t)$. Both have been smoothed and normalized in the same manner. **(A)** Traces of thumb, index, and little finger postion are shown for a 25 second period from the green electrode in subject 7. $C_1(t)$ (pink) and $H(t)$ (black) are shown beneath from the same period. **(B)** The correlation between traces of $C_1(t)$ and $H(t)$ with the paired movement from individual electrodes was calculated in the same manner as for figures 2 and 4 of the main text, and figure 7 of the supplement. Subjects 2 and 8 were excluded because they were not properly "tuned" (see figure 7). The similar structure and correlation between $C_1(t)$ and $H(t)$ suggests that the filtered high frequency power reasonably captures this broadband change.

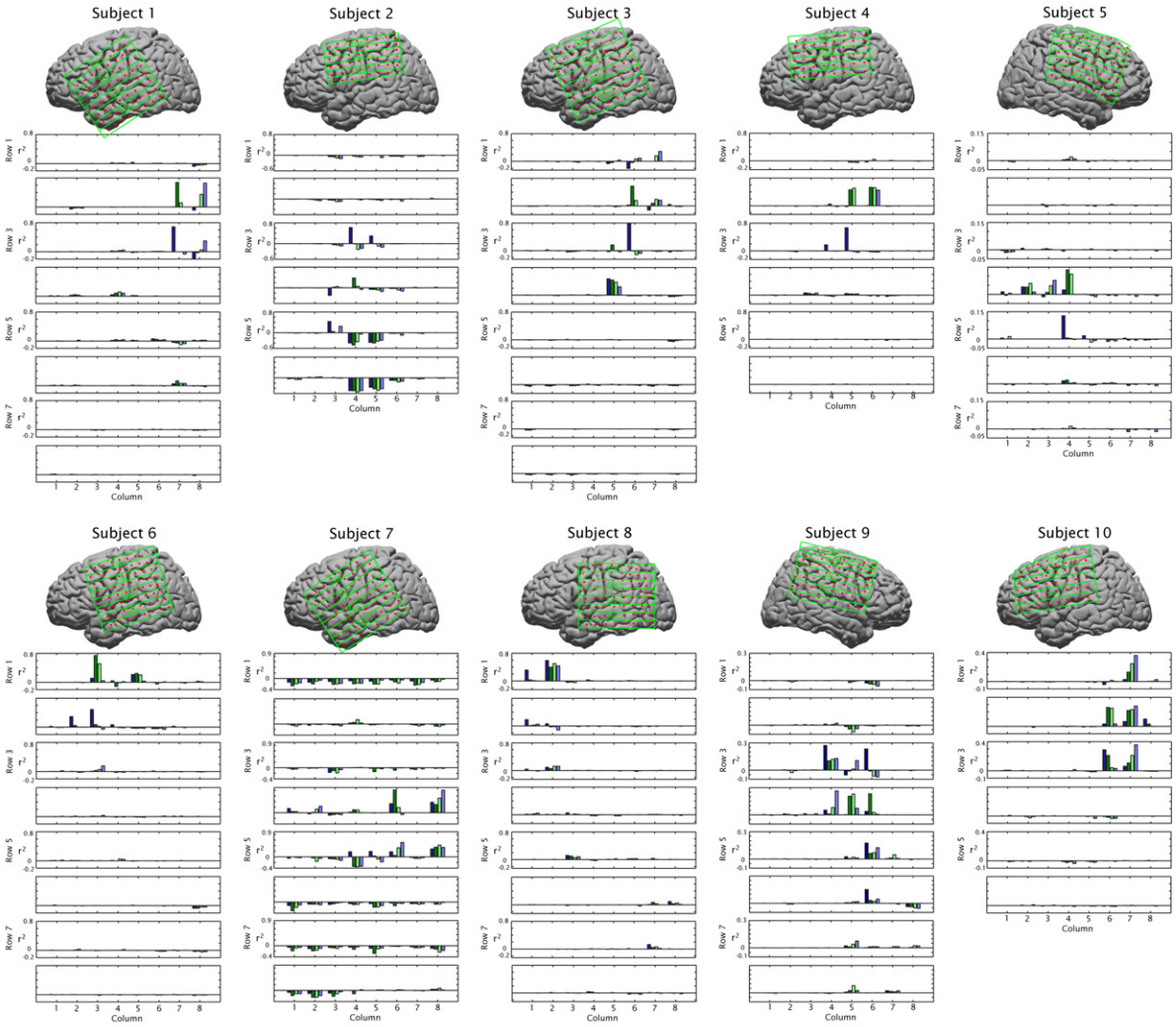

Figure S16: **Signed r^2 between movement samples and rest samples of the 1^{st} PSC, all electrodes in all subjects:** We plot the r^2 values for projection magnitude samples between movement and rest, for each movement independently. A negative sign was added when the mean value of rest samples was larger than movement samples. The colors for different movements are coded in the same manner as previous figures. The rows and columns correspond to rows (green) and electrode position (red) in the brain plot of each subject. This shows that few electrodes had significant change in each subject. The negative shift during all movement types, such as that seen diffusely in subject 7, indicates either augmentation of activity in rest intervals, or suppression of activity outside of motor areas during motor behavior.